AGU
ADVANCING
EARTH AND
SPACE SCIENCE

Geophysical Research Letters®

Key Points:

- Prediction uncertainties increase when the laser ablation energy of the training set spectra does not match the energy of the test set
- Over- or under-estimation of compositions are affected by ionization energies and peak distributions of individual elements
- The most accurate predictions are achieved when training set spectra encompass the range of laser energies in the spectra of unknowns

Correspondence to:
K. H. Lepore,
klepore@mtholyoke.edu

Effect of Plasma Temperature on Major Element Prediction Accuracy From Laser-Induced Breakdown Spectroscopy

K. H. Lepore[1] , M. D. Dyar[1,2] , and C. R. Ytsma[3,4]

[1]Department of Astronomy, Mount Holyoke College, South Hadley, MA, USA, [2]Planetary Science Institute, Tucson, AZ, USA, [3]Institute of Health Informatics, University College London, London, UK, [4]Cai Consulting, Glasgow, Scotland

Abstract Laser-induced breakdown spectra (LIBS) were collected on a diverse suite of ~2,600 geological standards using four laser energies (2.4–7.2 mJ) to assess how variations in irradiance from stand-off distance affect prediction accuracy. Mismatches in laser energies and plasma temperatures between training and prediction datasets introduce substantial uncertainty in major element predictions. For example, using 2.4 mJ spectra to predict 7.2 mJ data results in errors of ± 8.9, ± 1.4, ± 3.8, ± 3.2, ± 1.6, ± 1.0, ± 0.6, and ± 1.0 wt% for SiO_2, TiO_2, Al_2O_3, Fe_2O_3, MgO, CaO, Na_2O, and K_2O, respectively. When plasma temperatures of unknowns are represented in a multiple-plasma-temperature training set, prediction accuracies improve for the same oxides: ± 3.0, ± 0.3, ± 1.3, ± 1.4, ± 1.0, ± 0.7, ± 0.5, and ± 0.5 wt%. These results suggest that accuracies reported for Mars LIBS predictions based on single-distance, single laser-power calibration data may be overly optimistic except where Mars plasmas serendipitously match those acquired in the laboratory.

Plain Language Summary Laser-induced breakdown spectroscopy (LIBS) uses a laser to create a plasma on a sample surface. The spectrum of light emitted from this plasma is used to determine the composition of the target using atomic emission lines. Laser power alters the types of emissions represented in the plasma, and thus the observed spectra. A key question is whether the laser power of lab-based calibration spectra needs to match the laser power applied to unknown targets to understand their chemistry. A large reference collection of standards was sampled at a range of laser energies to examine effects of plasma fluctuations on quantitative measurements of chemistry. Models do a poor job of predicting sample chemistries when the plasma temperatures of calibration spectra do not match those of predicted targets. Comparatively, calibrations trained on a database of spectra covering a wide range of laser energies produce more accurate results for predicting unknowns at any energy within that range. Representation of possible plasma temperatures in training data is thus critical in LIBS calibrations, which are improved by sampling using a wide range of plasma conditions.

1. Introduction

The success of the ChemCam and SuperCam instruments onboard the *MSL Curiosity* and *Perseverance* rovers demonstrates the potential of laser-induced breakdown spectroscopy (LIBS) as an analytical tool (Wiens et al., 2013, 2020). In this technique, the laser creates a plasma with spectra consisting of emission lines from neutral, singly-, doubly-, and even triply-ionized species; these lines are then used to quantify chemistry.

A key source of variability in LIBS data is plasma temperature (Tokar et al., 2015); higher proportions of multiply-ionized lines are observed at higher temperatures. Plasma temperatures are largely determined by the energy density of the ablation laser on the target surface. In laboratory-based LIBS instruments, ablation parameters such as the focal length and target distance are kept constant, and the energy density on target can be adjusted by changing the energy of the laser beam.

The Mars missions cited above calibrated their instruments using spectra collected at a uniform distance and a single plasma temperature (Anderson et al., 2022; Clegg et al., 2017). It is now apparent that plasma temperatures vary widely in Mars spectra collected under a range of target distances due to changes in the ablation spot size (Maurice et al., 2012, 2021; Melikechi et al., 2014; Mezzacappa et al., 2016; Surmick et al., 2021). Mismatches between lab data and spectra of unknowns measured on Mars may result in degradation of geochemical accuracy.

This study determines if plasma temperatures must match among spectra collected for calibration purposes and those collected in the field for analytical analysis, and evaluates the consequences if they do not. Spectra collected
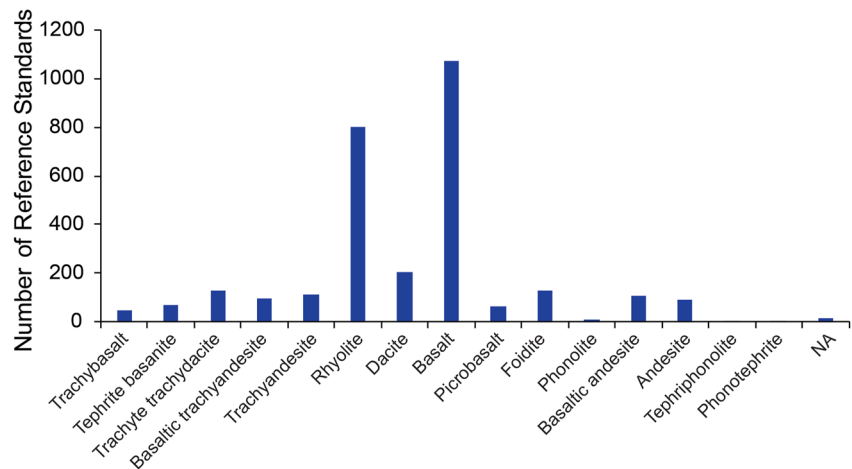
Figure 1. Distribution of rock types included in a geochemical reference database of 2,562 targets.

on ~2,600 geological standards at a range of laser energies mimic the effects of the changing ablation spot size observed on Mars. Multivariate models trained on spectra collected at each laser energy are used to predict major element compositions with test spectra collected at matched and mis-matched laser energies. This data set is used to assess the effects of matching/mismatching plasma temperature between calibrations and unknowns.

2. Materials and Methods

2.1. Reference Target Database

Reference targets include 2,562 rock powder standards collected from several sources as part of the Mars Fundamental Research program (Dyar et al., 2019). The distribution of rock types is approximately 70% igneous, 25% sedimentary, and 5% metamorphic (Figure 1). Included in this database are a series of rocks (from low-Si, high Mg-Fe basalts up to nearly pure SiO_2 sea sands) doped with trace elements of varying concentrations. These standards ensure that rock compositions encompass a range of surface materials anticipated on extraterrestrial bodies. Doped elements include Ba, C, Ce, Co, Cr, Cs, Cu, Ga, La, Li, Mn, Mo, Nb, Ni, Pb, Rb, S, Sc, Se, Sn, Sr, Y, Zn, and Zr in concentrations ranging from 100 ppm to 10 wt. %. Additional information on the major and minor element compositions of reference targets can be found in previous publications (Dyar et al., 2019; Lepore et al., 2022). Prior to LIBS analysis, rock powders with a ≪10 μm grain size were pressed into 1.6 cm diameter pellets under four tons pressure for 3 min, forming a flat, uniform sample surface.

2.2. Instrumentation

Spectra were collected on the SuperLIBS instrument in the Mineral Spectroscopy Laboratory at Mount Holyoke College using a Nd:YAG laser operating at 1,064 nm, 10 Hz, and a 7 ns pulse width. Laser energies ranged from 2.4 to 7.2 mJ on target, with a beam diameter of 110 μm. Plasma emission was separated into the UV (240–350 nm), VIS (370–480 nm), and VIS-NIR (508–870 nm) wavelength ranges and detected using two PIXIS cameras (UV and VIS) and a PI-MAX4 camera (VIS-NIR), each with 2D CCD detectors (e2v CCD42-10 back-illuminated high performance AIMO CCD sensors) identical to those on SuperCam on *Perseverance*. Spectral resolution is ~0.08 nm in the UV and VIS ranges, and ~0.40 nm in the VIS-NIR.

2.3. Spectra Collection

Samples were analyzed in 7 Torr CO_2 to mimic the atmospheric conditions on Mars. Spectra were collected on each target at four different laser energies (2.4, 4.0, 5.6, and 7.2 mJ) at five locations each. The lens-to-sample distance was constant throughout data collection. The range in laser energies resulted in laser fluences between 3.6 and 11 GW * cm^{-2}. Plasma emission was collected over a 10 ms interval to ensure that the entire lifetime of a single plasma was recorded during each integration. Thirty shots were recorded at each location; the first five
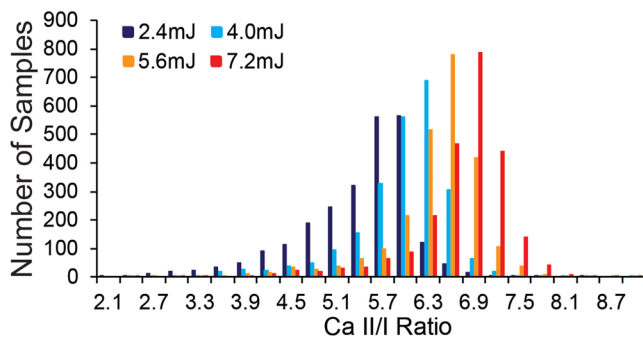
Figure 2. Histogram of the distributions of Ca(II)/Ca(I) ratios at 393.4 and 422.7 nm at each of four different laser energies used to generate a plasma on all reference targets.

shots were discarded to eliminate any contamination of the target surface. Spectra were averaged over 25 shots and five locations to produce a single spectrum for each reference target at each laser energy.

2.4. Spectra Processing

Data were preprocessed using a protocol similar to that used for ChemCam and SuperCam (Anderson et al., 2022; Wiens et al., 2013). Spectra were dark-subtracted, denoised, wavelength-aligned to a Ti standard, and corrected for instrument response. After preprocessing and before separating spectra into training and test sets for model analysis, spectra were masked to remove regions of the spectra with low instrument sensitivity. Baseline-correction used airPLS (Zhang et al., 2010). Normalization was performed independently for each wavelength range (UV, VIS, and VIS-NIR), analogous to the protocol used by the Mars instruments.

2.5. Analysis and Modeling Protocols

Data were analyzed using the Python Hyperspectral Analysis Tool (PyHAT) program developed by the USGS (Laura et al., 2022). Similar to SuperCam protocol, target outliers were identified using first-order predictions of major element compositions (Anderson et al., 2022). Spectral outliers (5% of data) were identified using an isolation forest protocol (Liu et al., 2012) to remove spectra that are very poorly predicted by multivariate models, likely due to sampling errors (pellet surface irregularities or contamination, e.g.,). Composition-based outliers were also identified from the concentrations of each major element using isolation forest, and an additional 5% of spectra were removed.

Spectra were separated into five folds, each representative of the composition range of each major element. One fold was held out as test spectra and remained unseen by the models trained on the remaining four folds. For all laser energies, samples in training and test sets for each major element were identical, ensuring consistency among datasets.

Cross-validation of partial least squares (PLS) models was used to identify the optimal number of components (from 2 to 30) for training. Compositions of the held-out test set spectra were predicted using the trained model and the accuracy and variance of the predicted compositions calculated (RMSE-P and r^2, respectively).

3. Results

3.1. Relationship Between Laser Energy and Plasma Temperature

Tokar et al. (2015) identified the ratio of the Si(II) peak at 634.7 nm to the Si(I) peak at 288.2 nm as a proxy for plasma temperature, which is impacted by laser-to-sample coupling to each sample as a function of composition, and the laser energy on target. Similarly, peak ratios can also be observed with ionized and neutral Ca peaks (393.4 and 422.7 nm, respectively) (Figure 2). Ionized and neutral peaks were selected from the same wavelength region in order to avoid disparities in peak area introduced during normalization. Substantial overlap among ratios at different laser energies is likely due to the wide range in sample composition. However, the clear trend toward higher ratios at higher laser energies demonstrates the relationship between laser energy and plasma temperature.

3.2. Training-Test Model Combinations

Five total PLS models were trained for each major oxide using spectra collected at each of four laser energies, as well as all energies combined into a single data set; in the latter case, there were four spectra for each target. To assess test accuracy, the held-out test spectra were separated by laser energy into four test sets for each element. An optimal scenario was run in which models trained at each laser energy were used to predict a matching test set. In addition, models trained on spectra collected at 2.4 and 7.2 mJ laser energy were used to predict spectra collected at 2.4, 4.0, 5.6, and 7.2 mJ.
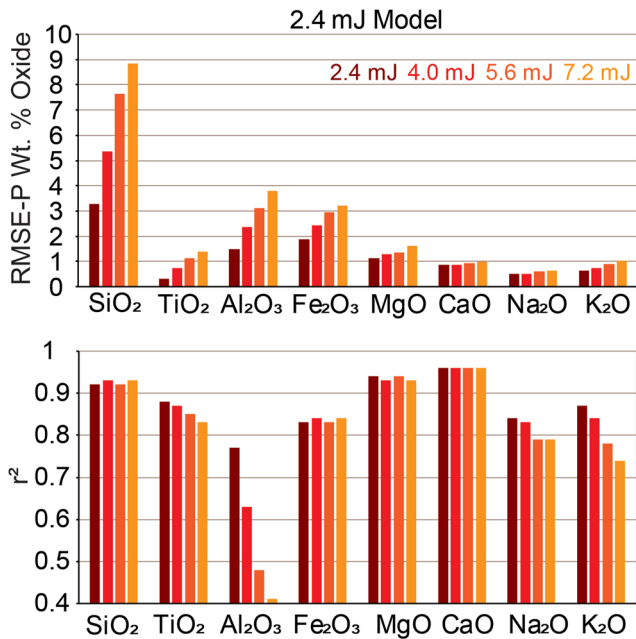
Figure 3. RMSE-P and r^2 values for models trained on spectra collected at 2.4 mJ and tested on spectra at each laser energy.

3.3. Models Trained Using One Laser Energy Used to Predict Other Laser Energies

PLS models trained using 2.4 mJ laser energy spectra were used to predict major elements using spectra acquired at each of the four energies (Figure 3). Prediction accuracies (RMSE-P) are worst when laser energies between training and test sets are most disparate. Accuracies improve as the plasma temperature of the test set approaches that of the training set. Similar trends are observed when 7.2 mJ laser energy models are tested (Figure 4). Dependence of accuracy on matching plasma temperatures was most pronounced for SiO_2, Al_2O_3, and Fe_2O_3. However, changes in the variance of predictions were most sensitive to plasma temperature changes for Al_2O_3, Na_2O, and K_2O.

3.4. Sensitivity of Different Elements to Plasma Temperature Variations

When the plasma temperatures for spectra in the training and test sets do not match, element predictions do not follow any specific trends. For example, SiO_2 is overestimated when a lower-temperature training set is used with a higher-temperature test set, and underestimated when the training set has a higher temperature (Figure 5). This trend is reversed for Al_2O_3, Fe_2O_3 and TiO_2.

These results likely relate to the different populations of ionization states present at varying temperatures. For example, Si displays prominent emission peaks at 288.2 nm for the neutral species and 634.7 and 637.1 nm for a singly-ionized species (Kramida et al., 2022). Training set spectra collected at lower plasma temperatures will have smaller Si (II) emission peaks than at high temperatures, resulting in a larger model coefficient. At a higher temperature, singly ionized species represented by the 634.7 nm peak will be more abundant, such that the model coefficients will be smaller relative to the coefficient at lower temperature. We hypothesize that this effect results in overprediction of SiO_2.
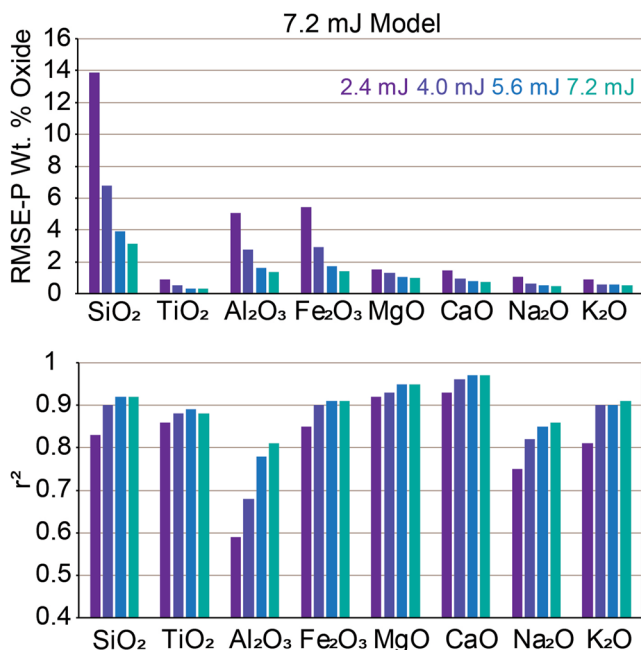
Ti and Fe have an abundance of ionized emission lines, particularly in the UV range. The energy transitions from neutral to singly-ionized states are lower for Ti and Fe (13.5755 and 16.19921 eV, respectively) than for Si (16.34585 eV). The abundance of lines and relatively low energy cost to transition to a higher ionization state indicate that models trained on lower temperatures might rely primarily on neutral or singly-ionized lines for predictions. When these models are applied to high-temperature test spectra that contain fewer low-energy transition lines in favor of higher ionization states, compositions might be underpredicted. Conversely, high-temperature trained models are still likely to utilize neutral and singly-ionized lines, which are enhanced relative to higher ionization states in low-temperature test spectra.

Al, like Si, has fewer emission peaks in the observed spectral range. Al also has the highest energy transition from the neutral to singly ionized state (18.82855 eV) and multivariate models are likely to rely heavily on (i.e., have large coefficients for) neutral Al emission lines, specifically the resonant Al peaks at 394.4 and 396.2 nm. The relatively low normalized peak intensities observed at high laser energies indicate substantial self-absorption of Al emission at these wavelengths (Figure 6). The high abundances of Al_2O_3 in geological materials, coupled with the fact that the most prominent lines are highly susceptible to self-absorption (Li et al., 2015; Mansour, 2015; Marpaung et al., 2022; Tang et al., 2020) indicate that low-temperature spectra are likely to overestimate the composition of Al_2O_3 when paired with
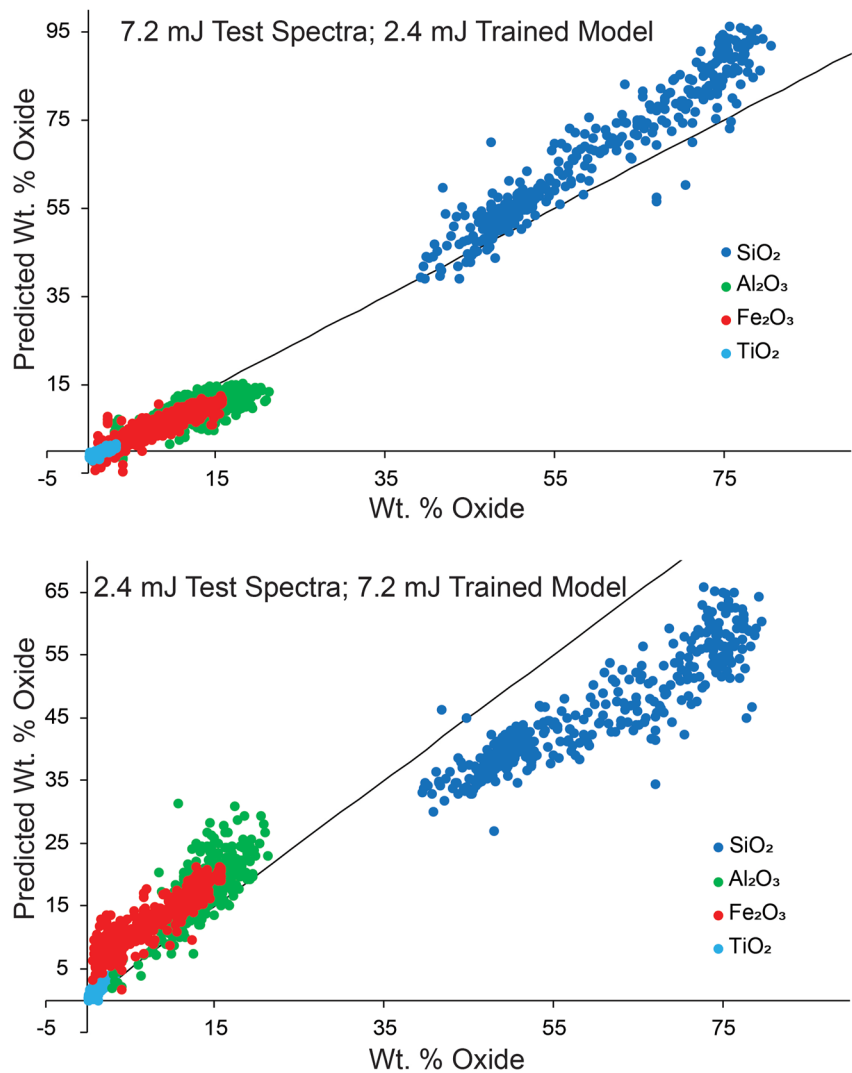

Figure 4. RMSE-P and r^2 values for models trained on spectra collected at 7.2 mJ and tested on spectra at each laser energy.

Figure 5. Predicted versus true concentrations of SiO_2, Al_2O_3, Fe_2O_3, and TiO_2 for two model conditions: a low-temperature trained model used to predict high-temperature test spectra, and a high-temperature trained model used to predict low-temperature test spectra.
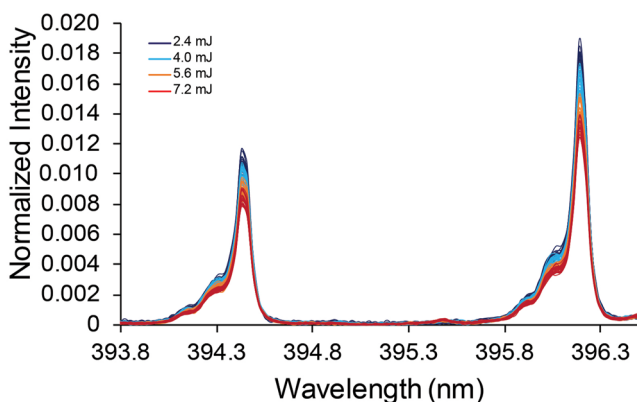

Figure 6. Normalized single-shot intensity spectra of resonant Al peaks collected on reference target G2 (basalt) show decreasing intensity with increasing laser energy.

high-temperature training spectra. This is corroborated by the increasing trend of Al_2O_3 predictions with distance reported by Wiens et al., 2021. No clear tendency to over- or underestimate is observed for MgO, CaO, Na_2O, or K_2O.

3.5. Prediction of Individual Spectra Using Multiple Plasma Temperature Training Sets

When spectra collected at all laser energies are combined into a single training set, prediction accuracies are nearly identical to those of the matched training-test predictions (Figure 7). Spectra used for training multivariate models should encompass the entire range of conditions that are present in test, or unknown, spectra to make accurate predictions. By including all laser energies into a single training set for each major element, PLS models are better at predicting compositions based on spectra collected under a range of plasma conditions, as seen here. This result supports that compiling multiple
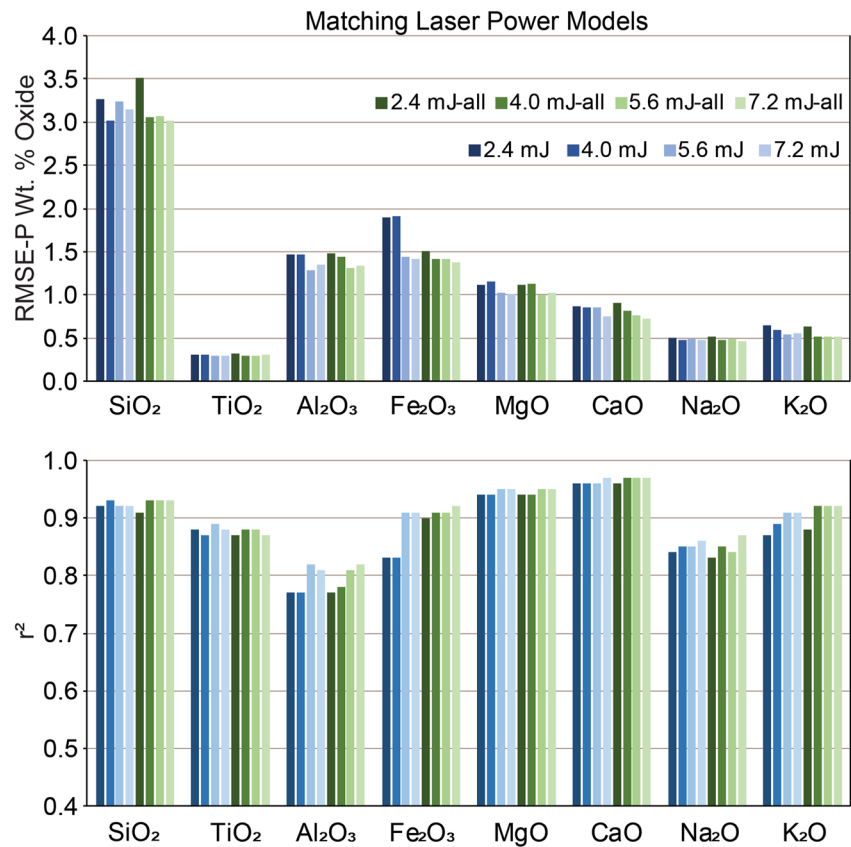
Figure 7. RMSE-P and r^2 values for predictions generated using single-energy training sets (blue bars) and combined laser energy training sets (green bars) with matching test set spectra.

plasma temperature data into one large, diverse model is superior to breaking calibration data into several submodels (here based on temperature, but also seen for compositions (Anderson et al., 2017; Lepore et al., 2022) and, more generally, data set size (Dyar & Ytsma, 2021)).

4. Conclusions

Discrepancies in laser energies and resultant plasma temperatures between training and test sets introduce a substantial amount of uncertainty in major element predictions. When plasma temperatures match, or when even a subset of spectra in the training set have matching plasma temperatures, prediction accuracies are greatly improved. Large, diverse calibration datasets produce the most reliable predictions, especially when target analyses are conducted under remote or variable conditions.

This result has important implications for calibration of in-situ instruments on planetary surfaces. It is understood that plasma temperatures vary widely in Mars spectra collected under a range of target distances due to changes in the ablation spot size (Melikechi et al., 2014; Mezzacappa et al., 2016; Surmick et al., 2021). Yet the calibration suites for both ChemCam and SuperCam were collected using a single stand-off distance and laser power (Anderson et al., 2022; Clegg et al., 2017). Because their reported accuracies for those missions depend on relatively simplistic lab calibrations, our results show that they are likely overly optimistic for spectra from Mars that are collected at different plasma temperatures. Recent attempts to mitigate the effect of decreasing plasma temperature with distance are complicated by a limited number of spectra collected at relevant distances, and the uncertainty introduced by relying on natural targets as standards with fixed composition (Wiens et al., 2021). The SuperLIBS instrument at Mount Holyoke uses spectrometers identical to those on *Perseverance*'s SuperCam; therefore the data set used here can be employed to predict Mars data with improved accuracy. Work is in progress in our group to apply the multi-laser-power calibration described in Figure 7 to Mars data using calibration

transfer in order to provide the community with alternative predictions for not only the major elements described here, but also for minor and trace elements.

Conflict of Interest

The authors declare no conflicts of interest relevant to this study.

Data Availability Statement

All spectra included in the research presented here are part of a larger LIBS reference database and will be made permanently available on the NASA Planetary Data System (PDS) Geosciences Node at https://doi.org/10.17189/b2aj-cz96. Data are expected to be openly available by mid 2023. In addition to future availability on PDS, spectra discussed in this paper can be found at https://doi.org/10.5281/zenodo.7566042. Software used for baseline removal, normalization, outlier detection, and multivariate modeling is publicly available (https://code.usgs.gov/astrogeology/PyHAT and https://github.com/ryanbanderson/PyHAT).

References

Anderson, R. B., Clegg, S. M., Frydenvang, J., Wiens, R. C., McLennan, S., Morris, R. V., et al. (2017). Improved accuracy in quantitative laser-induced breakdown spectroscopy using sub-models. *Spectrochimica Acta, Part B*, *129*, 49–57. https://doi.org/10.1016/j.sab.2016.12.003

Anderson, R. B., Forni, O., Cousin, A., Wiens, R. C., Clegg, S. M., Frydenvang, J., et al. (2022). Post-landing major element quantification using SuperCam laser induced breakdown spectroscopy. *Spectrochimica Acta, Part B*, *188*(2022), 106347. https://doi.org/10.1016/j.sab.2021.106347

Clegg, S., Wiens, R. C., Anderson, R., Forni, O., Frydenvang, J., Lasue, J., et al. (2017). Recalibration of the Mars Science Laboratory ChemCam instrument with an expanded geochemical database. *Spectrochimica Acta, Part B*, *129*, 64–85. https://doi.org/10.1016/j.sab.2016.12.003

Dyar, M. D., & Ytsma, C. R. (2021). Effect of data set size on geochemical quantification accuracy with laser-induced breakdown spectroscopy. *Spectrochimica Acta Part B: Atomic Spectroscopy*, *177*, 106073. https://doi.org/10.1016/j.sab.2021.106073

Dyar, M. D., Ytsma, C. R., & Lepore, K. H. (2019). Standards for geochemical analysis of major, minor, and trace elements in rock powders. In *Lunar and planetary science*. Lunar and Planetary Institute. (abstr.#1396).

Kramida, A., Ralchenko, Y., & Reader, J., & NIST ASD Team. (2022). *NIST atomic spectra database*, ver. 5.10. National Institute of Standards and Technology. https://doi.org/10.18434/T4W30F. Retrieved from https://physics.nist.gov/asd

Laura, J. R., Gaddis, L. R., Anderson, R. B., & Aneece, I. P. (2022). Introduction to the Python Hyperspectral Analysis Tool (PyHAT). In *Machine learning for planetary science*. Elsevier. https://doi.org/10.1016/B978-0-12-818721-0.00012-4

Lepore, K. H., Ytsma, C. R., & Dyar, M. D. (2022). Quantitative prediction accuracies derived from laser-induced breakdown spectra using optimized multivariate submodels. *Spectrochimica Acta, Part B*, *191*, 106408. https://doi.org/10.1016/j.sab.2022.106408

Li, J.-M., Guo, L.-B., Li, C.-M., Zhao, N., Yang, X.-Y., Hao, Z.-Q., et al. (2015). Self-absorption reduction in laser-induced breakdown spectroscopy using laser-stimulated absorption. *Optics Letters*, *40*(22), 5224–5226. https://doi.org/10.1364/OL.40.005224

Liu, F. T., Ting, K. M., & Zhou, Z.-H. (2012). Isolation-based anomaly detection. *ACM Transactions on Knowledge Discovery from Data*, *6*(1), 1–39. https://doi.org/10.1145/2133360.2133363

Mansour, S. A. M. (2015). Self-absorption effects on electron temperature-measurements utilizing laser induced breakdown spectroscopy (LIBS)-techniques. *Optics and Photonics Journal*, *5*(03), 79–90. https://doi.org/10.4236/opj.2015.53007

Marpaung, A. M., Harefa, E., Pardede, M., Karnadi, I., Hedwig, R., Tanra, I., et al. (2022). Simple defocus laser irradiation to suppress self-absorption in laser-induced breakdown spectroscopy (LIBS). *Heliyon*, *8*, e10057. https://doi.org/10.1016/j.heliyon.2022.e10057

Maurice, S., Wiens, R. C., Bernardi, P., Cais, P., Robinson, S., Nelson, T., et al. (2021). The SuperCam instrument suite on the Mars 2020 rover: Science objectives and mast-unit description. *Space Science Reviews*, *217*(47), 3–108. https://doi.org/10.1007/s11214-021-00807-w

Maurice, S., Wiens, R. C., Saccoccio, M., Barraclough, B., Gasnault, O., Forni, O., et al. (2012). The ChemCam Instrument Suite on the Mars Science Laboratory (MSL) rover: Science objectives and mast unit description. *Space Science Reviews*, *170*(1–4), 95–166. https://doi.org/10.1007/s11214-012-9912-2

Melikechi, N., Mezzacappa, A., Cousin, A., Lanza, N. L., Lasue, J., Clegg, S. M., et al. (2014). Correcting for variable laser-target distances of laser-induced breakdown spectroscopy measurements with ChemCam using emission lines of Martian dust spectra. *Spectrochimica Acta, Part B*, *96*, 51–60. https://doi.org/10.1016/j.sab.2014.04.004

Mezzacappa, A., Melikechi, N., Cousin, A., Wiens, R. C., Jasue, J., Clegg, S. M., et al. (2016). Application of distance correction to ChemCam laser-induced breakdown spectroscopy measurements. *Spectrochimica Acta, Part B*, *120*, 19–29. https://doi.org/10.1016/j.sab.2016.03.009

Surmick, D. M., Taleh, L., & Melikechi, N. (2021). Effects of laser beam focusing characteristics on laser-induced breakdown spectra. *Applied Spectroscopy*, *75*(2), 127–136. https://doi.org/10.1177/0003702820961437

Tang, Y., Ma, S., Yuan, R., Ma, Y., Sheng, W., Zhan, S., et al. (2020). Spectral interference elimination and self-absorption reduction in laser-induced breakdown spectroscopy assisted with laser-stimulated absorption. *Optics and Lasers in Engineering*, *134*, 106254. https://doi.org/10.1016/j.optlaseng.2020.106254

Tokar, R. L., Wiens, R. C., Maurice, S., Pilleri, A., Gellert, R., Anderson, R. B., et al. (2015). Relationship between MSL/ChemCam laser focus, plasma temperature, and compositional calibrations. In *Lunar and planetary science XLVI*. Lunar and Planetary Institute. (abstr.#1369).

Wiens, R. C., Blazon-Brown, A. J., Melikechi, N., Frydenvang, J., Dehouck, E., Clegg, S. M., et al. (2021). Improving ChemCam LIBS long-distance elemental compositions using empirical abundance trends. *Spectrochimica Acta, Part B*, *182*(2021), 106247. https://doi.org/10.1016/j.sab.2021.106247

Wiens, R. C., Maurice, S., Lasue, J., Forni, O., Anderson, R. B., Clegg, S., et al. (2013). Pre-flight calibration and initial data processing for the ChemCam laser-induced breakdown spectroscopy instrument on the Mars Science Laboratory rover. *Spectrochimica Acta, Part B*, *82*, 1–27. https://doi.org/10.1016/j.sab.2013.02.003

Wiens, R. C., Maurice, S., Robinson, S. H., Nelson, A. E., Cais, P., Bernardi, P., et al. (2020). The SuperCam instrument suite on the NASA Mars 2020 rover: Body unit and combined system tests. *Space Science Reviews*, *217*(1), 4. https://doi.org/10.1007/s11214-020-00777-5

Zhang, Z.-M., Chen, S., & Liang, Y. Z. (2010). Baseline correction using adaptive iteratively reweighted penalized least squares. *Analyst*, *135*(5), 1138–1146. https://doi.org/10.1039/b922045c